JOURNAL OF MATERIALS SCIENCE 4 (1969) 290–301

# Fluxoid Pinning by Second Phases in a Superconducting Niobium-Zirconium Alloy

G. W. J. WALDRON*
*The General Electric Company Limited, Central Research Laboratories, Hirst Research Centre, Wembley, UK*

*Received 18 July 1968, and in revised form 10 October*

The effects of second phases on the critical currents of superconducting niobium-zirconium alloys containing a nominal 25 wt % zirconium have been determined by superconducting magnetisation experiments. Heat treatment of annealed and extruded materials in the temperature range 600 to 900° C leads to a cellular decomposition of the high temperature $\beta$ structure into two isostructural phases, one niobium-rich ($\beta_{Nb}$) and the other zirconium rich ($\beta_{Zr}$), with an accompanying increase in critical current (at an average field of 20 kOe) up to twelve times the original value. Heat treatment of quenched tubes at 800 or 900° C produces precipitation on sub-boundaries prior to the cellular reaction, this being accompanied by an increase in critical current to at least thirteen times the original value. In this case, however, prolonged heating leads to a fall in critical current which it is suggested is an "overageing" effect.

## 1. Introduction

Many superconducting metals and alloys are capable of carrying small currents in the superconducting state, that is without developing electrical resistance. When a given, rather low, value of current (the critical current, which varies from one material to another) is exceeded, such superconductors are driven normal, and then develop small but detectable levels of electrical resistance. There is a certain class of superconductors, however, some of which are able to carry large currents in high magnetic fields without being driven normal. These are known as Type II superconductors. A few Type II materials remain capable of carrying appreciable current densities in fields beyond 100 kOe, and are thus of great commercial importance.

A magnetic field will always exist in a superconducting material carrying current, even if only the self field of the current, in the absence of an external field. When a current flows in the material the lines of magnetic flux (known as fluxoids in a Type II superconductor) are subject to a Lorentz force analogous to the well known force on a conductor carrying current in a magnetic field. The superconductor will remain capable of carrying high currents only if some means is found of slowing the resulting motion of the fluxoid array. Otherwise the movement of fluxoids generates heat which drives the superconductor normal.

It is now believed that structural defects (e.g. small angle dislocation boundaries) and second phases are capable of pinning fluxoids [1-4], thus leading to high critical currents in Type II superconductors. Many experiments have been carried out, however, in which there was insufficient control over metallurgical variables to enable the effect of one kind of defect to be differentiated from that of another. For instance, it is generally accepted that severe cold working (such as occurs in wire drawing) is necessary to produce high current-carrying capacity in the commercial high-field superconductor Nb—25% Zr. This is often attributed to the high dislocation density produced by cold working, but the material can also contain stringers of second-phase which could be effective as fluxoid pinners. Point defects produced during the working process could also be important. It is obviously difficult to correlate the current-carrying properties of a drawn wire or a rolled strip with the complex and

*Now at: British Rail Engineering Laboratories, London Road, Derby, England.

highly distorted structures of these materials. This difficulty becomes even more acute when the wire or strip is heat treated. Heat treatment of severely worked Nb—25% Zr can lead to point defect migration (and possible clustering) and annealing, formation of sub-structure, precipitation and recrystallisation. Furthermore, at least two of these processes (sub-structure formation and precipitation) are known to interact [5]. Obviously, it is desirable to begin with simpler structures before correlation between superconducting properties and microstructure is attempted.

Livingston [6-8] has carried out experiments with lead alloys which clearly differentiate the effects of dislocations and second phases as fluxoid pinners, and this work has clarified the effects of chemical and structural inhomogeneities in Type II superconductors. Up to the present, no similar work has been reported on the class of superconductors capable of carrying high currents in high magnetic fields. In this investigation, Nb—25% Zr has been examined. Apart from its commercial importance, this material can be produced in the single or multi-phase conditions. According to the Rogers and Atkins phase diagram [9] at equilibrium the high temperature $\beta$ separates below about 910° C into two isostructural bcc phases, a niobium-rich phase ($\beta_{Nb}$) and a zirconium-rich phase ($\beta_{Zr}$), whilst below the monotectoid horizontal at 610° C a two-phase ($\beta_{Nb} + \alpha_{Zr}$) field exists. Hence it seemed possible to induce fluxoid pinning in Nb—25% Zr by heat treatment which would produce a dispersion of pinners (e.g. $\beta_{Zr}$) in a superconducting matrix ($\beta_{Nb}$). The Nb—25% Zr has been used mostly in conditions of heat treatment which obviate the complication of a worked structure, but experiments have also been performed on material in the as-extruded condition. Additional heat treatment has been carried out in the range 500 to 900° C. Metallographic and X-ray studies have been correlated with superconducting tube magnetisation measurements. The more detailed metallurgical aspects of the work will be described elsewhere, although results of relevance are quoted in the present paper.

## 2. Experimental Method

### 2.1. Specimen Preparation

Two batches of material whose analyses are given in table I, have been used in the present work. One of these, Batch 1 (B1), was double electron-beam melted stock originating from the USA. It was obtained in the form of a $\frac{1}{2}$ in. diameter extruded rod, but details of its preparation were not available. Batch 2 (B2), was supplied by IMI Ltd, Witton. Here, a 2 in. diameter arc-melted ingot was extruded at 1050° C to 1 in. diameter and then to $\frac{1}{2}$ in. diameter at the same temperature. Tube specimens (18 to 20 mm × 5 mm OD × 1 mm bore) were machined from both batches of Nb—25% Zr rod for tube magnetisation experiments (see below), the tube axes being cut parallel to the rod axis. A single larger tube of B1 material (10.4 mm OD × 1 mm bore) was also prepared. A further set of tube specimens of dimensions 18 to 22 mm × 3 mm OD × 1 mm bore was cut from B2 material for quenching experiments.

Tubes of the two as-received materials were sealed off individually in quartz capsules under a vacuum of about $5 \times 10^{-4}$ torr, and heated at temperatures in the range 500 to 900° C for up to 300 h. Furnace temperatures were controlled to ± 2 to 3° C, and tubes were inserted and withdrawn while the furnaces were at tempera-

TABLE I Analysis of nominal Nb—25% Zr materials used in the present work.

| Batch and treatment | Zr wt % | O ppm | C ppm | N ppm | H ppm |
|---|---|---|---|---|---|
| B1 annealed | 26.9* | 75 90 109 | 50 | 13 9 8 | 9 7 9 |
| (grain size 30 μm) | 27.3† 27.3 | 106 95 74 | 20 | 17 5 9 | 7 6 8 |
| | 27.3* | 49 60 75 | 60 | 7 5 6 | 9 5 8 |
| B2 as-extruded | 23.3 | 163 162 206 | 100 | 52 40 38 | 11 13 9 |
| (grain size 5 μm) | 22.0† 22.1 | 260 285 242 | 150 | 31 12 23 | 10 10 9 |
| | | 575 559 | 160 | 19 38 | 4 8 |
| B2 quenched from 1500° C (grain size 30 to 50 μm) | No analysis | | | | |

*Determined by X-ray fluorescence spectroscopy using the chemically-analysed specimens as reference standards.
†Determined chemically.

ture. The series of 3 mm diameter tubes was given a homogenising treatment of 1 h at 1500° C under a dynamic vacuum of about $10^{-5}$ torr and then quenched into silicone oil. These quenched tubes were also subsequently heat treated in evacuated and sealed quartz capsules.

### 2.2. Magnetisation Experiments

The tube magnetisation experiment of Kim, Hempstead and Strnad [10] has been used to evaluate the fluxoid pinning properties of Nb—25% Zr. In this experiment, an external magnetic field ($H_E$) applied parallel to the axis of a superconducting tube specimen is increased, and the field inside the tube ($H_I$) is monitored. Initially $H_I$ remains at zero, because shielding currents are set up in the wall of the tube which oppose the applied field. Microscopically, pinning points are hindering the motion of fluxoids and causing a fluxoid density gradient, so that the circulating currents of the fluxoids integrate to a finite value.

When the external field reaches a critical value, the average current density in the wall of the tube is a maximum for that field and any further increase in external field causes flux penetration into the bore and an increase in internal field. Theoretically this increase (a penetration curve in fig. 1) follows a hyperbolic relation, as does the curve corresponding to decreasing external

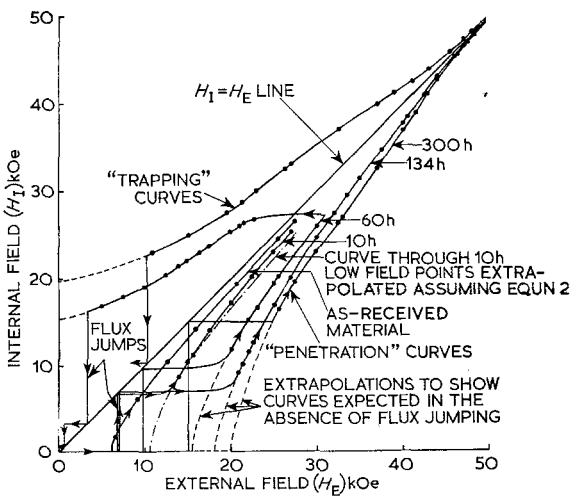


*Figure 1* Effect of heat treatment at 800° C on the field penetration curves of B1 tubes.

field (a trapping curve in fig. 1). Using the Maxwell relation

$$\text{curl } H = 0.4\pi J \qquad (1)$$

and assuming a relation

$$J(H + H_0) = \alpha_c \qquad (2)$$

it has been shown that [10] for tube specimens

$$0.4\,\pi\, w\alpha_c = M(H^* + H_0) \qquad (3)$$

where $J$ = current density (A/cm²), $H$ = field (kOe), $w$ = tube wall thickness (cm), $M$ = mod $|H_E - H_I|$ (kOe), $H^* = \frac{1}{2}(H_E + H_I)$ (kOe), $\alpha_c$ = a material constant (kOe $M$A/cm²), $H_0$ = another material constant. $\alpha_c$ gives a measure of the flux pinning ability of a material by measuring its current carrying capacity. An increase in $\alpha_c$ corresponds to a transposition of the penetration curve to the right and of the trapping curve to the left, that is away from the 45° line ($H_E = H_I$) in either case (fig. 1). Furthermore, the average current density in the wall of the tube is given by

$$J_c = M/0.4\pi w \qquad (4)$$

In the present work, the external field was supplied by a 54 kOe $\frac{1}{2}$ in. bore superconducting solenoid, and the internal field was monitored by a copper magnetoresistance probe. The specimen was held firmly in place (although liquid helium was allowed to circulate freely) in a "Tufnol" specimen holder inserted into the bore of the solenoid, the latter being contained in a double-walled stainless steel dewar. All superconducting measurements were made at 4.2° K. The solenoid power supply enabled the current, and hence the field, to be varied smoothly at controlled rates. The positions of the penetration and trapping curves were not dependent on field sweep rate, although a low rate (1.8 kOe/min) was normally used.

### 2.3. Metallurgical and X-ray Examination

After the tube magnetisation measurements had been carried out, a section perpendicular to the axis was taken from each tube, mounted, polished, etched and examined using conventional metallographic techniques. Electron microscope replicas were also taken from the polished surface.

Phases present prior to and after heat treatment were determined by: (a) a reflection X-ray diffraction technique; (b) X-ray powder diffraction on residues obtained by a solvent extraction method described by Laverty and Hiltz [11].

## 3. Results

### 3.1. Batch 1 Material

The as-received B1 material followed the hyperbolic $H_I$ versus $H_E$ behaviour following from the assumptions in [10] up to at least 27 kOe (fig. 1). The $\alpha_c$ value of the as-received material was low, about 0.1 kOe $M$A/cm², and its microstructure

was recrystallised and was virtually single-phase, apart from a trace of a grain-boundary reaction.

Heat treatment in the temperature range 600 to 800° C markedly increased the current-carrying capacity of the tubes (figs. 1 and 2). Improvements also occurred at 500° C, but very much more slowly. In contrast, on heat treatment at 900° C, $\alpha_c$ fell.

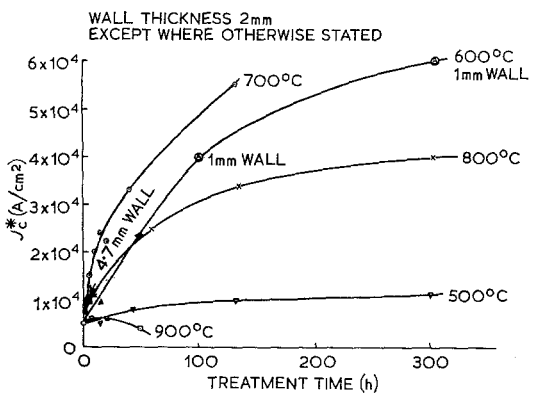


*Figure 2* Effect of heat treatment on the critical currents of B1 tubes ($H^* = 20$ kOe).

Where there was an increase in $J_c$ at low fields, the phenomenon of flux jumping [12] appeared (fig. 1). Repeated flux jumping occurred at low values of external field for high values of initial $J_c$, but died out at higher fields. Other deviations from idealised behaviour also appeared: beyond an external field of 15 to 20 kOe, the current-carrying capacity of the tubes fell below that predicted (by the formula in [10]) from the initial penetration behaviour (e.g. 10 h 800° C curve, fig. 1). Consequently, since $\alpha_c$ is no longer a constant, values of average current density in the wall of the tube, rather than $\alpha_c$, have mostly been used here as a measure of the flux pinning capability of the material (fig. 2), although some low $\alpha_c$ values are also quoted. $J_c$ values at low field after extended periods of heat treatment have been estimated by extrapolating back into the field region where flux jumps occurred.

$J_c$ for a given $H^*$ was obtained from a plot of $M$ versus $H^*$, using equation 4. $M$ values were derived for both increasing and decreasing external fields, both sets of values lying to a good approximation on a common curve. The "average" $J_c$ thus arrived at, is referred to as $J_c^*$.

The effect on the low-field $J_c^*$ of B1 material of varying the temperature of heat treatment is shown in fig. 2. Metallographic examination shows that the increase in $J_c^*$ at a given temperature in the range 600 to 800° C coincides with a cellular decomposition of the $\beta$-phase into $\beta_{Nb}$ and $\beta_{Zr}$ (fig. 3). At 900° C, the $\beta \rightarrow \beta_{Nb} + \beta_{Zr}$ decomposition is slow, and the $\beta_{Zr}$ formed is as coarse as the small amount present in the as-received material. A grain-boundary reaction also occurs at 500° C, but has not been identified. The rate of this reaction is again extremely slow.

In considering the $J_c^*$ versus $t$ relations of fig. 2 it is instructive to examine in addition plots of per cent reaction versus time of heat treatment and $J_c^*$ versus per cent reaction (figs. 4 and 5). Considering fig. 4 first, the rate of reaction at 800° C is about the same as that at 700° C, but that at 600° C is much slower; this behaviour is due to the sigmoidal kinetics of the decomposition [13] and will be discussed elsewhere. Nevertheless, as fig. 5 now shows, in spite of the similarity in the 700 and 800° C transformation rates, for a given percentage transformation, the current density at low fields is always greater after heat treatment at 700 than at 800° C: the extrapolated value of $J_c^*$ for 100% transformation is about $6.0 \times 10^4$ A/cm² (for $H^* = 20$ kOe) at 700° C and about $3.8 \times 10^4$ A/cm² at 800° C. The current-carrying capacity after transformation at 600° C is higher than at either of the other temperatures; for 100% transformation $J_c$ (for $H^* = 20$ kOe) would be about $8.0 \times 10^4$ A/cm².

The phase decomposition illustrated in fig. 3 progressively transforms a matrix of $\beta$-phase with a reasonably high upper critical field ($H_{c2} = 70$ to 80 kOe) and with a low density of fluxoid pinning points, into a matrix of $\beta_{Nb}$ with a rather low $H_{c2}$ (about 50 kOe, the precise value depending on the temperature of reaction) containing a high density of pinning points. The latter consist of $\beta_{Zr}$ with an $H_{c2}$ of about 100 kOe.

Values of $H_{c2}$ for phases in the Nb—Zr system have been estimated by first deducing compositions from the Rogers and Atkins phase diagram [9] and then using the known $H_{c2}$ versus composition relationship for Nb—Zr alloys [14, 15]. The X-ray lattice parameter determinations in the present work roughly confirm the published $\beta_{Nb}$ compositions, although they indicate that there is a spread of compositions a few per cent either side of the nominal figures. The $\beta_{Zr}$ equilibrium compositions are not reached, however, the $\beta_{Zr}$ being richer in niobium than would be expected from the phase

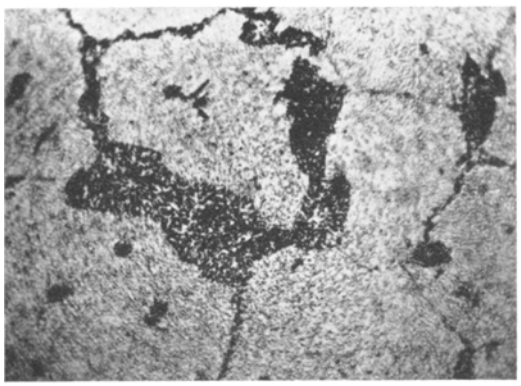

(a)

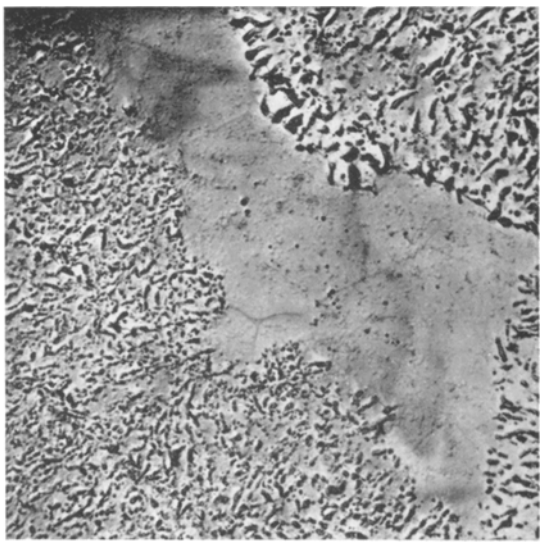

(b)

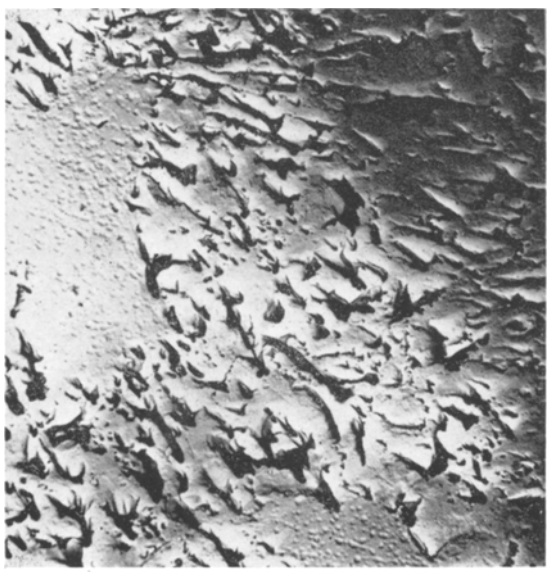

(c)

*Figure 3* Cellular transformation of single-phase $\beta$ into duplex ($\beta_{Nb} + \beta_{Zr}$) due to heat treatment of B1 material (a) 15 h 700° C × 1000; (b) 130 h 700° C × 4000; (c) 134 h 800° C × 4000.

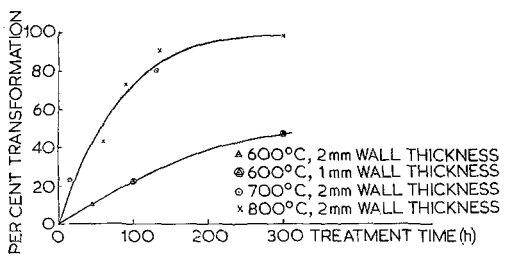


*Figure 4* Rates of cellular transformation for different temperatures, B1 material.

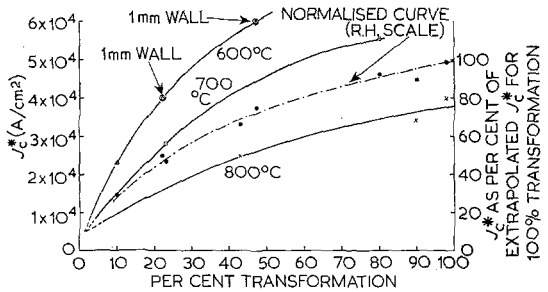


*Figure 5* Variation of $J_c^*$ ($H^* = 20$ kOe) with extent of cellular transformation for different temperatures, B1 material. Sample wall 2 mm except for two points.

diagram. At 700° C, for instance, it contains about 40% Nb, instead of the 22% equilibrium value. Unfortunately it has not been possible to determine the composition of the $\beta_{Zr}$ formed at 600° C directly by X-ray diffraction, but the failure to reach equilibrium would be expected to be more marked at the lower temperature. The equilibrium $\beta_{Zr}$ composition at 800° C contains 30 to 35% zirconium. However, the value of $H_{c2}$ is not too sensitive to zirconium content in the

zirconium-rich alloys except at high zirconium values (> about 75%), so the $\beta_{Zr}$ formed in the temperature range 600 to 800° C will probably all have an upper critical field of about 100 kOe.

Returning now to fig. 3, since the cellular reaction initiates at grain-boundaries, the ($\beta_{Nb}$ + $\beta_{Zr}$) duplex cells become multiply-connected at an early stage in the process. It is thus not expected that there will be a direct proportionality between the extent of the reaction and the current-carrying capacity of the tubes [16]. The heat treated materials contain closed circuits of ($\beta_{Nb}$ + $\beta_{Zr}$) transformation products, which apparently trap more fluxoids (and hence support higher critical currents) than would be expected from the amounts of transformation which occur. This is particularly noticeable in the early stages of the $\beta$-decomposition, when the effects of multiple-connectivity are first apparent. The importance of the topology of the $\beta$-decomposition in determining critical currents is further illustrated by the dashed curve in fig. 5: the $J_c$* values for the three temperatures of heat treatment all lie close to this common curve after normalisation with respect to their values at 100% transformation.

The fall-off in $J_c$* at high fields can cause crossing of the penetration ($H_E$ versus $H_I$) curves for different times at a given temperature. For example, in the 600° C series, beyond $H^* \simeq 30$ kOe, the 100 h tube carries more current than the 300 h tube; at $H^* = 40$ kOe, for instance, $6.0 \times 10^3$ A/cm$^2$ compared with $3.2 \times 10^3$ A/cm$^2$.

### 3.2. Batch 2 Material

The critical current of the as-received B2 material at low fields was higher than that of B1, corresponding to an initial $\alpha_c$ of 0.2 to 0.3 kOe $MA/cm^2$. As in B1 material with the same current-carrying ability, equation 2 was not followed beyond about 20 kOe. The effect of heat treatment at 600 to 800° C was also similar to that in B1 material, producing marked increases in current-carrying capacity at low fields (fig. 6).

The as-received B2 material has a stringered structure, with recrystallisation commencing in the $\beta_{Nb}$ matrix. Figure 7a shows a section perpendicular to the stringer direction. X-ray diffraction examination of chemical residues indicates that the stringers consist of a mixed carbide, (Zr, Nb) C. The stringer structure is presumably responsible for the higher initial $\alpha_c$ of B2 material as compared with B1. Heat treatment causes $\beta$-phase splitting to occur at the stringers and particularly at the grain-boundaries, as shown in figs. 7b and 7c. In contrast with B1 there is no marked variation in the scale of dispersion of $\beta_{Zr}$ with temperature in B2 specimens, except in the few tubes heat treated at 900° C. The cause of this is uncertain, but it may be due to the presence of appreciable amounts of carbon and oxygen in the B2 material affecting

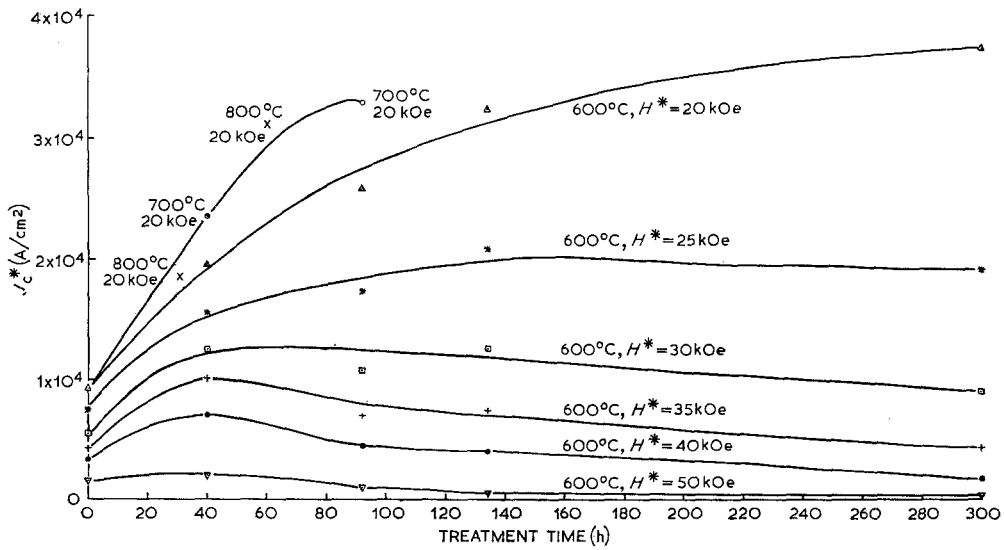


*Figure 6* Effect of heat treatment on the critical currents of B2 tubes ($H^*$ = 20 kOe).

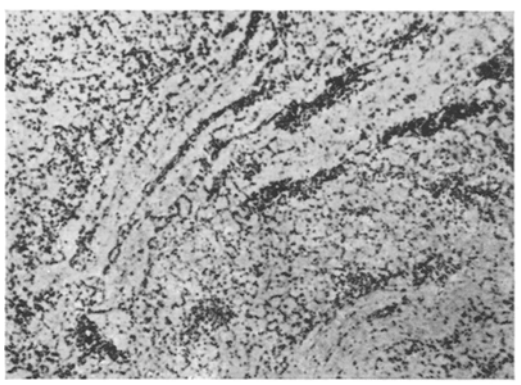

(a)

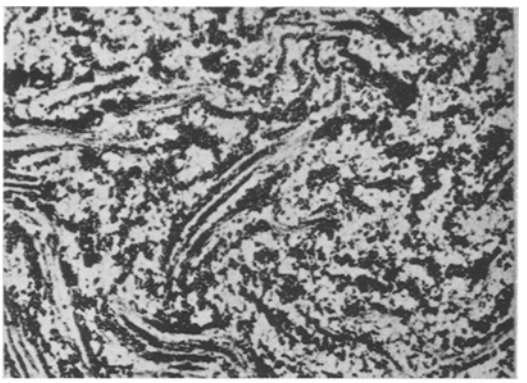

(b)

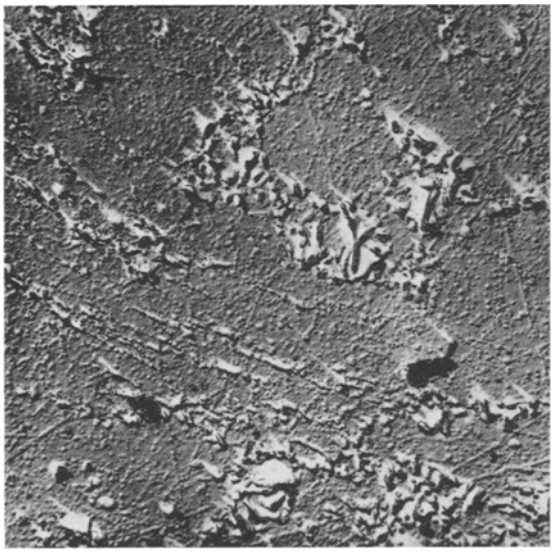

(c)

*Figure 7* (a) As-received B2 material, tube cross-section × 500; (b) B2 material, 300 h 600° C × 300; (c) B2 material, 40 h 700° C × 4000.

nucleation and growth. In tubes heated at 900° C, spheroidisation and growth of the second-phase particles occurs, and the critical current actually falls with increasing time of heat treatment.

The high-field behaviour of B2 tubes after heat treatment at 600° C has been examined, although no attempt has been made to pin-point critical times of heat treatment (fig. 6). At $H^* = 25$ kOe, a broad maximum develops which becomes more localised at higher fields and moves to shorter times of heat treatment.

### 3.3. Quenched Material

The current-carrying ability of the as-quenched tubes was low (figs. 8, 9), corresponding to an $\alpha_c$ of only about 0.05 kOe $M$A/cm$^2$. Equation 2 was followed up to the maximum $H_E$ of the magnet, 54 kOe. Figure 10a shows that the microstructure of the material was substantially single-phase $\beta$, although in electron micrographs particles of what was probably the mixed carbide (Zr, Nb) C could be seen at grain-boundaries.

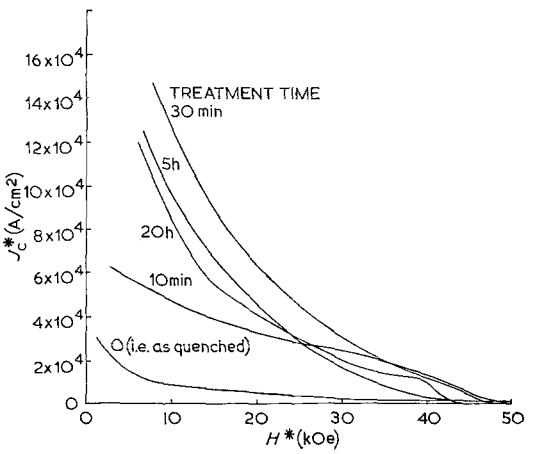


*Figure 8* Effect of 900° C heat treatment on the critical current versus field curves for tubes quenched from 1500° C.

Heat treatment at 700° C produced very little change in $J_c^*$: even 20 h at 700° C gave only a small increase, and there was no corresponding change in microstructure. However, marked changes in current-carrying capacity were produced by heat treatment at 800 and 900° C. In contrast to the behaviour of the as-received B1

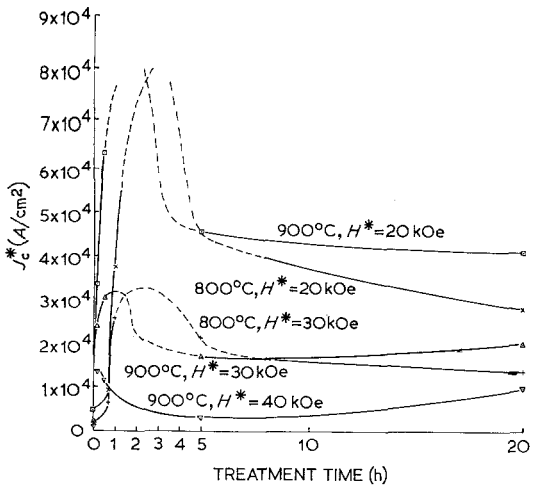


*Figure 9* Effect of heat treatment on the critical currents of tubes quenched from 1500° C.

and B2 materials, though, the initial large increase in $J^*$ at low fields (fig. 9) were not accompanied by the discontinuous pearlitic-type $\beta$-phase decomposition noted previously (figs. 3, 7). After 30 min at 900° C and 5 h at 800° C, precipitation on sub-boundaries could be detected (fig. 10b). Only for longer times of heat treatment when $J_c^*$ had fallen from its peak value did the grain-boundary pearlitic mode of $\beta$-phase decomposition occur to any extent (fig. 10c). Obviously, the kinetics of the $\beta \rightarrow \beta_{Nb} + \beta_{Zr}$ transformation in the quenched material are different from those in either the B1 or B2 tubes, as will be discussed elsewhere [23].

As the critical currents of the tubes were increased by heat treatments, deviations from equation 2 appeared. After 40 min at 800° C, equation 2 was satisfied up to about 40 kOe, but

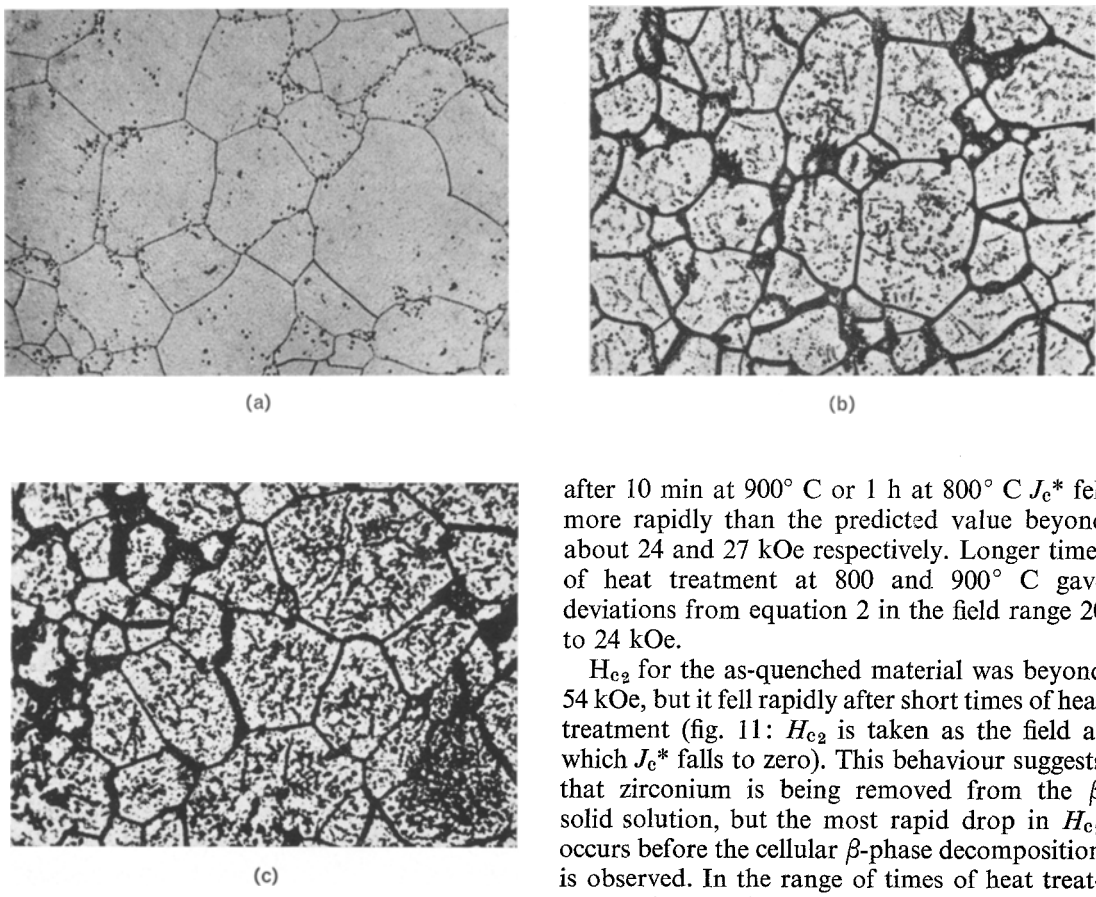


*Figure 10* (a) Tube quenched from 1500° C × 300; (b) Tube quenched from 1500° C, then heat treated 30 min at 900° C × 300. (c) Tube quenched from 1500° C, then heat treated 5 h at 900° C × 300.

after 10 min at 900° C or 1 h at 800° C $J_c^*$ fell more rapidly than the predicted value beyond about 24 and 27 kOe respectively. Longer times of heat treatment at 800 and 900° C gave deviations from equation 2 in the field range 20 to 24 kOe.

$H_{c2}$ for the as-quenched material was beyond 54 kOe, but it fell rapidly after short times of heat treatment (fig. 11: $H_{c2}$ is taken as the field at which $J_c^*$ falls to zero). This behaviour suggests that zirconium is being removed from the $\beta$ solid solution, but the most rapid drop in $H_{c2}$ occurs before the cellular $\beta$-phase decomposition is observed. In the range of times of heat treatment when it does occur, the fall in $H_{c2}$ is relatively small. It seems likely that both the initial rapid increase in $J_c^*$ and initial rapid fall in $H_c^*$ are due to precipitation, occurring pre-

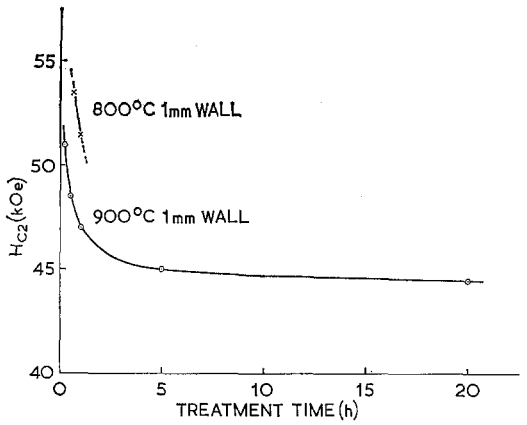


*Figure 11* Effect of heat treatment on $H_{c_2}$ for tubes quenched from 1500° C.

ferentially at sub-boundaries within the $\beta$-grains. The nature of this precipitation will be discussed in another paper. The size of the precipitate is at first too small to be resolved by the replica technique. As precipitate growth occurs with increasing time of heat treatment, an optimum size is attained which produces maximum pinning. It is at about this stage that precipitation within grains is detected (fig. 10b), although even then only the largest particles in a range of sizes (which are least effective as pinners) are being seen.

For sizes of precipitate greater than this, pinning becomes less effective and an "overageing" effect is evident (fig. 9). In this range of ageing times (30 min to 20 h at 900° C, 5 to 20 h at 800° C) the $\beta \rightarrow \beta_{Nb} + \beta_{Zr}$ grain-boundary cellular decomposition occurs (fig. 10c), and must also contribute to the current-carrying capacity of the tubes. For short periods of heat treatment (say 10 min at 900° C or 1 h at 800° C), increases in $J_c$* occur at all fields up to about 50 kOe (fig. 8). After 30 min at 900° C, however, the corresponding $J_c$* versus $H$* curve falls to just below that for 10 min at 900° C beyond 36 kOe. Overageing causes the curve for 5 h at 900° C to lie below that for 30 min at 900° C at all fields. After 20 h at 900° C, due to the appreciable amount of the $\beta \rightarrow \beta_{Nb} + \beta_{Zr}$ cellular reaction which has taken place, the $J_c$* versus $H$* curve rises above the 5 h at 900° C curve beyond about 24 kOe. At both 800 and 900° C, the time of heat treatment at which the maximum $J_c$* value occurs becomes shorter as $H$* increases (fig. 9).

## 4. Discussion

It has been shown in the present work that high critical current densities can be produced in Nb—25% Zr initially containing low dislocation densities (B1 and quenched materials), by heat treatments which cause second phases to form.

In B1 material, the low-field (20 kOe) values of $J_c$* extrapolated to 100% transformation increase from about $3.8 \times 10^4$ A/cm$^2$ to about $8 \times 10^4$ A/cm$^2$ as the temperature of heat treatment is reduced from 800 to 600° C. This can be ascribed to variations in: (a) the scale of dispersion of $\beta_{Zr}$ and $\beta_{Nb}$; (b) the chemical compositions and relative proportions of the $\beta_{Nb}$ and $\beta_{Zr}$ formed at the three temperatures of heat treatment.

Discussing now the importance of these factors, the interparticle spacings [1] at 600 and 700° C are about the same (0.2 $\mu$m), and are much smaller than at 800° C ($\sim 1\mu$m, fig. 4). The smaller the spacing the closer it approaches a critical value ($l_{crit} \sim 10^{-6}$ cm for Nb—25% Zr), the significance of which is more conveniently discussed below when dealing with the results from the quenched tubes. Optimum pinning and hence maximum $J_c$ is expected when $1 \simeq l_{crit}$.

The variation in composition of the $\beta_{Nb}$ with temperature of heat treatment leads to a fall in the value of $H_{c_2}$ as the temperature is lowered and hence to a corresponding fall in the Ginsberg-Landau parameter $\kappa$, since

$$\kappa = H_{c_2}/\sqrt{2}\, H_c \qquad (5)$$

and $H_c$ (the thermodynamic critical field) remains roughly constant as the composition changes. It has been shown [20] that in Pb—11.6 % Sn—10% In, for a given precipitate distribution (coarser than that to give optimum pinning, i.e. $1 > l_{crit}$) the critical current rises as the matrix $\kappa$ is lowered.

It has been suggested in section 3.1. that all the $\beta_{Zr}$ formed in the range 600 to 800° C had an upper critical field of about 100 kOe. Since the $H_{c_2}$ of the $\beta_{Zr}$ is always higher than that of the $\beta_{Nb}$, pinning will be relatively weak [21].

Comparing now the behaviour of the tubes heat treated at 600 and 700°C, the much higher critical currents of the 600° C series are rather surprising. The range of $\beta_{Zr}$ particle sizes and spacings formed at the two temperatures is similar; the upper critical fields of the two $\beta_{Nb}$ compositions differ by only 5 kOe (corresponding to a 10% difference in $\kappa$), and the slightly

higher volume fraction of pinning material formed at 600° C is not expected to be important. A topological phenomenon may be responsible, since there is some evidence from the electron micrographs that the $\beta_{Zr}$ formed at 600° C tended to be more interconnected than that at 700° C.

Comparing next the 700 and 800° C series, the higher critical currents of the former are likely to be predominantly due to the finer scale of the $\beta_{Zr}$ dispersions. In the first place, the difference in the $H_{c2}$ values of the $\beta_{Nb}$ at the two temperatures of heat treatment is only about 10 kOe, which is too small to account for the differences in $J_c$* values. Furthermore, in the B2 materials, where there is no well-defined difference between the size and spacing of the $\beta_{Zr}$ formed in the temperature range 600 to 800° C, the 700 and 800° C curves coincide (fig. 6). The relative positions of the low field $J_c$* versus $t$ relations for B1 and B2 materials (B1 higher at 600 and 700, but lower at 800° C) can be qualitatively explained in terms of the $\beta_{Zr}$ particle size and distribution, but it must also be remembered that the interstitial contents of the two materials are quite different (table I). A further illustration of the effect of size and spacing of pinning particle on critical current is given by the 900° C series in both B1 and B2 materials: the coarse particles (diameter about 1 to 2 $\mu$m, spacing 2 $\mu$m) formed give rise to low critical currents.

The overageing effect in the $J_c$ versus $t$ curves of the quenched tubes (fig. 9) is strong evidence for second-phase pinning. Analogous behaviour occurs during the heat treatment of certain age-hardening alloys, when the value of a mechanical property such as yield stress first increases, passes through a maximum, then falls off. This effect is also due to growth of a second-phase to and then beyond a critical size [22]. It was thus of interest to examine the variation of current-carrying capacity of the quenched tubes with size and spacing of the second-phase pinning material. Unfortunately, the lower limit of measured interparticle spacings in the present replica work was a few hundred Å. As a result, near the maximum of the $J_c$* versus $t$ curves for 20 kOe in fig. 9, individual particles were not resolved, although for times beyond the maxima, interparticle spacings in the range 0.05 to 0.1 $\mu$m were measured. Following Anderson and Kim [4], we expect the critical current of a hard superconductor at a given field to be inversely proportional to the mean distance between pinning centres, 1. There will be a limiting value of 1 below which the pinning force, and hence the critical current is expected to fall again: this may be approximately equal to the coherence length $\xi$. A further proposal is that pinning will be most effective when the spacing of pinning centres is related to the fluxoid spacing, $d$, at the given field value. This means that the size and distribution of pinning points to produce most effective pinning will vary with field. There is some evidence for this in the results from the quenched tubes. Assuming a triangular fluxoid assembly and one quantum of flux, $2 \times 10^{-7}$ G cm$^2$, per flux line, $d$ is approximately 0.05 $\mu$m at 10 kOe, about the same as the upper limit of the distance between pinning centres found to give maximum $J_c$*. Furthermore, the time of heat treatment maximising $J_c$* becomes shorter as $H_c$* increases (fig. 9), which suggests that as the fluxoids pack more closely, the pinning centres of smaller dimensions and smaller interparticle distance are becoming most effective as fluxoid pinners. The slower changes in $J_c$* occurring at 800° C reflect the thermally-activated nature of the growth of pinning points.

It is noteworthy that in the as-quenched (single-phase) material, equation 2 holds rather well up to an external field of 54 kOe, whereas in the heat treated (two-phase) material, deviations from this relation occur in a field range which falls to lower field values as the time of heat treatment is increasingly prolonged. This supports the notion of precipitation induced by heat treatment causing a new type of pinning centre to form, which is implicit in the above discussion of pinning in the quenched tubes. Similar effects are produced by heating as-received B1 and B2 tubes. In these specimens, however, the original structure contains some second-phase material, so that a deviation from the above relation is obvious in the $H_{int}$ versus $H_{ext}$ curves for the as-received alloys. Furthermore, the details of the variation in pinning with heat treatment are different in the three materials examined, since the precipitation modes are different.

The $J_c$* versus $t$ curves for fields above 20 kOe for the B2 600° C series show maxima, which become more localised and move to lower values of $t$ as $H$* increases to 40 kOe (fig. 6). This behaviour is probably a further result of the $\beta \rightarrow \beta_{Nb} + \beta_{Zr}$ cellular decomposition (section 3.1.) which has already been discussed in some detail. As the value of $H$* approaches the $H_{c2}$ of

the $\beta_{Nb}$ matrix of the duplex $\beta_{Nb} + \beta_{Zr}$ structure, the $J_c$* of the tube falls as soon as an appreciable amount of the cellular reaction has occurred. The closer the value of $H$* is to the $H_{c2}$ of the $\beta_{Nb}$, the sooner is the critical range of $t$ reached. It is significant that at $H^* = 50$ kOe, the maximum in the $J_c$ versus $t$ relation has almost disappeared: the $H_{c2}$ of the $\beta_{Nb}$ is at about this field. The few results available at high values of $H$* for the B1 tubes heat treated at 600° C suggested that a similar effect occurs in that material (section 3.1.).

The present work has shown that the $\beta_{Zr}$ produced by heat treatment of Nb—Zr alloys of about the 25% Zr composition is not an effective flux pinner at high fields. This is because (a) the $\beta_{Zr}$ is a superconducting pinning phase with an upper critical field higher than that of the $\beta_{Nb}$ matrix; (b) the $\beta_{Nb}$ matrix has relatively low values of upper critical field.

## 5. Conclusions

(1) In superconducting magnetisation experiments, single-phase $\beta$ Nb—25% Zr has a low critical current, and follows the relation derived in [10]

$$J(H + H_0) = \alpha_0$$

up to fields beyond 50 kOe. When its critical current is increased by heat treatment, however, the range of field over which the relation in [10] is obeyed is reduced, and flux jumping appears in the low-field range.

(2) Heat treatment of recrystallised Nb—25% Zr in the temperature range 600 to 900° C causes a cellular decomposition of single-phase $\beta$ into two isostructural bcc solid solutions, one niobium-rich ($\beta_{Nb}$) and the other zirconium-rich ($\beta_{Zr}$). The $\beta_{Zr}$, although itself a superconductor, acts as a fluxoid pinning phase in the matrix of $\beta_{Nb}$. Values of critical current at an average field of 20 kOe can be raised by a factor eight to twelve by the heat treatment, the increase being greatest at 600° C.

(3) In an as-extruded material containing a stringer structure, critical currents at low fields are increased by heat treatment generally as in the recrystallised Nb—25% Zr, although details of the variation of $J_c$ with temperature of heat treatment are different. At high fields (> 20 kOe) maxima develop in the critical current versus time of heat treatment curves.

(4) Quenching from the single-phase $\beta$ region at 1500° C affects behaviour during subsequent heat treatment. Initially, sub-boundary precipitates form and grow. Concurrently critical current values increase and pass through a maximum (at least thirteen times greater than the as-quenched value) before falling again. This ageing phenomenon demonstrates the existence of a critical size and dispersion of pinning centre to produce optimum pinning.

(5) In the heat treated tubes, critical currents fall to low values at high fields. This is because: (a) $\beta_{Zr}$ is a relatively poor fluxoid pinner because its upper critical field is higher than that of the matrix; (b) the matrix $\beta_{Nb}$ has a relatively low upper critical field.

## Acknowledgement

This work formed part of a collaborative research programme supported by the Ministry of Technology.

The chemical analysis, electron microscopy, solvent extraction work and X-ray diffraction described in this report were carried out by members of the Chemistry and Technical Services Division, Hirst Research Centre, to whom the author's thanks are due. The author would also like to express his appreciation to fellow members of the Superconductivity Group at the Centre for useful discussions and help with the experimental phase of the work, and in particular to Mr M. Williams for his advice and encouragement.

## References

1. J. FRIEDEL, P. G. DEGENNES, and J. MATRICON, *Appl. Phys. Lett.* **2** (1963) 119.
2. J. SILCOX and R. W. ROLLINS, *Appl. Phys. Lett.* **2** (1963) 231.
3. W. W. WEBB, *Phys. Rev. Lett.* **11** (1963) 191.
4. P. W. ANDERSON and Y. B. KIM, *Rev. Mod. Phys.* **36** (1964) 39.
5. M. S. WALKER, R. STICKLER, and F. E. WERNER, "Metallurgy of Advanced Electronic Materials", edited by Brock (Interscience, New York, 1962) p. 49.
6. J. D. LIVINGSTON, *Acta Metallurgica* **11** (1963) 1371.
7. *Idem, Phys. Rev.* **129** (1963) 1943.
8. *Idem, J. Appl. Phys.* **34** (1963) 3028.
9. B. A. ROGERS and D. F. ATKINS, *Trans. AIMME* **203** (1955) 1034.
10. Y. B. KIM, C. F. HEMPSTEAD, and A. R. STRNAD, *Phys. Rev.* **129** (1963) 528.
11. D. P. LAVERTY and R. H. HILTZ, "Advances in X-ray Analysis", **8** (Plenum Press, New York, 1965) p. 103.
12. N. MORTON, *Phys. Lett.* **19** (1965) 457.
13. G. R. LOVE and M. L. PICKLESIMER, *Trans. Met. Soc. AIME* **236** (1966) 430.

14. K. M. RALLS, A. L. DONLEVY, R. M. ROSE, and J. WULFF, "Metallurgy of Advanced Electronic Materials", edited by Brock (Interscience, New York, 1962) p. 35.
15. H. T. COFFEY, J. K. HULM, W. T. REYNOLDS, D. K. FOX, and R. E. SPAN, *J. Appl. Phys.* **36** (1965) 128.
16. J. D. LIVINGSTON and H. W. SCHLADER, *Progr. Matls. Sci.* **12** (1963-5) 183.
17. H. J. LEVINSTEIN, E. S. GREINER, and H. MASON, JR, *J. Appl. Phys.* **37** (1966) 164.
18. A. V. NARLIKAR and D. DEW-HUGHES, *J. Materials Sci.* **1** (1966) 317.
19. J. P. MCEVOY and R. F. DECELL, *J. Appl. Phys.* **35** (1964) 982.
20. J. D. LIVINGSTON, *Rev. Mod. Phys.* **36** (1964) 54.
21. T. H. ALDEN and J. D. LIVINGSTON, *Appl. Phys. Lett.* **8** (1966) 6.
22. A. KELLY and R. B. NICHOLSON, *Progr. Matls. Sci.* **10** (1963) 151.
23. G. W. T. WALDRON, *J. Less Common Met.* **17** (1969) 167.